Available online at www.sciencedirect.com
SCIENCE DIRECT®
Journal of Crystal Growth 274 (2005) 265–280
JOURNAL OF CRYSTAL GROWTH
www.elsevier.com/locate/jcrysgro

Delayed onset of return flow by substrate inclination in model horizontal longitudinal MOCVD processes

W.S. Kuo[a], C.Y. Wang[a], J.L. Tuh[b], T.F. Lin[a,*]

[a]*Department of Mechanical Engineering, National Chiao Tung University, Hsinchu, Taiwan 30010, ROC*
[b]*Department of Air-conditioning and Refrigeration Engineering, Chin Min Institute of Technology, Miaoli, Taiwan 351, ROC*

Received 23 June 2004; accepted 24 September 2004
Communicated by K. Nakajima
Available online 23 November 2004

Abstract

In this study an experimental flow visualization is carried out to investigate how the substrate inclination affects the buoyancy-induced return flow structure in mixed convection of gas in a horizontal rectangular duct. The return flow is driven by a heated circular disk embedded in the bottom plate of the duct, simulating that in a horizontal longitudinal MOCVD reactor. Specifically, the bottom plate of the duct is inclined so that the gas flow in the duct is accelerated, causing the buoyancy-to-inertia ratio to decrease in the main flow direction. In the experiment, the Reynolds and Rayleigh numbers of the flow at the duct inlet are respectively varied from 3.7 to 79.7 and from 9040 to 24,000 for the inclined angle of the bottom plate fixed at 0°, 0.34° and 0.97°. Particular attention is paid to delineating the spatial changes of the return flow structure with the plate inclination angle and to how the bottom plate tilting possibly suppresses and stabilizes the flow. The results show a substantial delay in the onset of the return flow and the effective suppression of the buoyancy-driven unstable vortex flow by the bottom plate inclination. Besides, the bottom plate inclination can effectively weaken the return flow at slightly higher Reynolds numbers. An empirical equation is provided to correlate the present data for the onset of the return flow in the duct with its bottom inclined at 0° and 0.97°.

Keywords: A1. Convection; A2. Fluid flows; A3. Metalorganic chemical vapor deposition

1. Introduction

Buoyancy-driven vortex flow and the associated thermal characteristics in mixed convective gas flow through a horizontal plane channel heated from below recently receive increasing attention because of the important role they play in the

*Corresponding author. Tel.: +886 35 712121 55118; fax: +886 35 726 6 440.
E-mail address: tflin@mail.nctu.edu.tw (T.F. Lin).

0022-0248/$ - see front matter © 2004 Elsevier B.V. All rights reserved.
doi:10.1016/j.jcrysgro.2004.09.097

Nomenclature

A	aspect ratio of duct, b/d
b	channel width
d	channel height at the duct inlet
g	gravitational acceleration
Gr	grashof number, $g\beta d^3(T_{in}-T_{cp})/v^2$
Pr	prandtl number, v/α
Ra	rayleigh number, $\beta g d^3\Delta T/\alpha v$
Re	reynolds number, $W_m\, d/v$
Gr/Re^2	buoyancy-to-inertia ratio
T	temperature
T_{in}, T_{cp}	gas temperature at inlet of test section and temperature of copper plate
ΔT	$T_{cp}-T_{in}$
t	time, s
W_m	mean velocity of gas in axial direction
X, Y, Z	dimensional cartesian coordinates
x, y, z	dimensionless cartesian coordinates scaled with b, d, l

Greek

α	thermal diffusivity
β	thermal expansion coefficient
γ_{crit}	critical buoyancy-to-inertia ratio
v	kinematic viscosity
ϕ	inclined angle of the bottom plate measured from the horizontal

horizontal metal organic chemical vapor deposition (MOCVD) processes for thin crystal film growth. It is well known that the buoyancy-driven vortex flow can result in a non-uniform vapor deposition on silicon wafers and is harmful to the thin film properties [1]. At sufficiently high buoyancy-to-inertia ratios [2] the buoyancy-driven vortex flow can even become unstable. Moreover, at high buoyancy the forced flow can be reversed resulting in a return flow zone in the channel. The return flow will cause a memory effect in the MOCVD processes. This memory effect is detrimental to the epitaxial layer and should be avoided. In order to eliminate or weaken the vortex and return flows, the conventional method which is widely used in the industry is to reduce the cross-sectional area of the channel in the streamwise direction. Reduction of the channel cross-section by the substrate inclination can accelerate the forced flow so that the buoyancy-to-inertia ratio in the flow decreases in the streamwise direction. This was found to be very effective in suppressing the buoyancy-induced temporal flow oscillation in MOCVD processes. But the details on how the vortex and return flows are affected by the substrate inclination remain largely unexplored. In a recent model experiment [3], we examined the buoyancy-driven 3-D return flow pattern in a gas flow over a heated circular disk embedded in the bottom plate of a horizontal rectangular duct, simulating that in a horizontal longitudinal MOCVD reactor. Here in the present study, we move further to investigate how the buoyancy-driven return flow is affected by the substrate inclination.

In the mixed convective flow through a bottom heated flat duct, the return flow is known to result from the strong upward thermal buoyancy as the cold entering gas is suddenly heated in the entry-heated section of the duct. The cold flow from the upstream is forced to lift up first and moves obliquely upward. Then, the flow is blocked to move upstream by the strong retarding force of the upward buoyancy, forming a reverse flow zone. At high buoyancy the return flow can penetrate significantly into the upstream unheated section of the duct and becomes highly elongated. When the main flow is at a high Reynolds number, the return flow can extend substantially into the heated section of the duct and is also highly elongated.

The return flow encountered in the horizontal MOCVD reactors was first investigated by Eversteyn et al. [4] by visualizing the flow. They identified a particle-free zone above the susceptor and erroneously interpreted this zone as a stagnant layer of fluid. Instead, it is well known today as the return flow zone. Kamotani et al. [5] experimentally examined the thermal instability of a laminar flow in a horizontal flat duct heated from below

and found that at a high buoyancy-to-inertia ratio with $Gr/Re^2 \gg 1$ a reverse flow zone was induced near the upper plate. Flow visualization conducted by Giling [6] to investigate flow pattern and temperature profile in horizontal MOCVD reactors proved that there was no stagnant layer above the susceptor. According to the experimental and numerical study of nitrogen and hydrogen gas flows in a bottom-heated quartz reactor with a rectangular cross-section, Visser et al. [7] indicated that the returning flow was mainly dominated by two dimensionless parameters, the Grashof and Reynolds numbers, Gr and Re. They proposed a critical level γ_{crit} for the mixed convection parameter Gr/Re^{κ} and showed that no return flow occurred when $Gr/Re^{\kappa} < \gamma_{crit}$. The exponent κ is equal to 1 at low Reynolds numbers ($Re \leqslant 4$) and goes to 2 at higher Reynolds numbers ($Re \geqslant 8$). A similar study from Fotiadis et al. [8] also indicated that either the heated susceptor was placed in the bottom or top wall a flow recirculation could be induced. Moreover, the recirculation was noted in the upper portion of the reactor.

A 2-D numerical simulation carried out by Ouazzani et al. [9] to predict the buoyancy driven flow recirculations in the entrance region of a horizontal MOCVD reactor manifested that the presence of the return flow could result in an increase of film growth rate at the leading edge of the substrate and a decrease in the downstream. Later, they [10] extended the analysis to include the 3-D effects and found that at a high Ra/Re ratio, a buoyancy-induced reverse flow existed in the transition region between the isothermal entrance and the reaction section. Einset et al. [11] moved further to define the onset of recirculation flows in the entrance region of horizontal CVD reactors based on the relative magnitudes of the vertical and horizontal pressure gradients in the flow. The pressure effects are independent of whether the heated substrate faces up or down, which explains their experimental observation that the flow recirculations appear at the same position in either configuration. Besides, they noted that the recirculation rolls located near the top wall of the reactor and rotated counter-clockwisely for both top- and bottom-heated reactors. Ingle and Mountziaris [12] again used a 2-D numerical simulation to investigate the onset of transverse buoyancy-driven circulations in a horizontal flat duct consisting of a cool upstream section, a middle section with a heated bottom wall, and a cool downstream section. Their results showed a transverse recirculation formed in the middle section near the top wall above the leading edge of the hot bottom wall, which rotated in a counter-clockwise direction. The other one formed near the bottom wall above the exit end of the hot bottom plate and rotated in a clockwise direction. At increasing inlet velocity, the downstream transverse recirculation was eliminated first and the upstream one shrank significantly. In addition, they proposed two criteria for the absence of the transverse recirculaton as $(Gr/Re^2) < 100$ for $10^{-3} < Re \leqslant 4$, and $(Gr/Re^2) < 25$ for $4 \leqslant Re < 100$. A similar 2-D numerical simulation from Ingham et al. [13,14] predicted that the transverse flow recirculation could extend to the upstream of the wall temperature discontinuity. The onset of the return flow for the heated lower wall was shown to occur at $Gr/Re^2 \cong 17$ for $Re = 10$. This critical value of Gr/Re^2 slowly decreased at increasing Re. Besides, the recirculation zone is larger for a lower Re. Makhviladze and Martjushenko [15] conducted 2-D and 3-D numerical simulations to study the return flow in horizontal bottom wall heated CVD reactors. They showed the formation mechanism of the return flow and the return flow could be suppressed by cooling the side walls and/or by reducing the width of the reactors. The characteristics of 3-D flow, heat and mass transfer in a horizontal CVD reactor were numerically investigated by Park and Pak [16]. They concluded that for a large Gr/Re^2 the return flow appeared at the leading edge of the susceptor, and it caused an increase in the growth rate of the film at this region and a decrease in the downstream of the susceptor. Recently, the 3-D return flow structure driven by a heated circular disk embedded in the bottom wall of a rectangular duct was examined by Tuh and Lin [3] through experimental flow visualization.

A simple mean often used to suppress and stabilize the buoyancy-driven vortex flow is to accelerate the forced flow, as demonstrated by Chen et al. [17]. Gau et al. [18] revealed that in a convergent channel with the top plate inclination,

the acceleration of the forced flow could delay the onset of thermal instability and effectively suppress the temperature fluctuation. Tseng et al. [19] experimentally showed that inclining the top plate of a rectangular duct uniformly heated from below could effectively and completely wipe out the irregular temporal flow oscillation. But the induced vortex flow can only be weakened to some degree. Besides, more vortex rolls would be induced due to the increase in the aspect ratio of the duct in the mean flow direction.

The above literature review clearly indicates that how the buoyancy-induced return flow is affected by the substrate inclination remains largely unexplored in horizontal MOCVD reactors. An experimental flow visualization is conducted here to explore the effects of the substrate inclination on the return flow in a horizontal rectangular duct with a heated circular disk embedded in the duct bottom, simulating that in a horizontal longitudinal reactor.

2. Experimental apparatus and procedures

The experimental system established in the previous study [3,20] is also used here with a slight modification of the test section. Fig. 1 shows a schematic of the present experimental apparatus designed to investigate the effects of the substrate inclination on the buoyancy-induced return flow and the adopted coordinate system. To reduce the cost of the experiment, we use air as the working fluid to replace the inert gases normally employed in real MOCVD processes. In view of the similar thermophysical properties for various gases, the results obtained here are still applicable to the MOCVD systems.

The apparatus begins with the air regulated from a 300 l and 100 psi high-pressure tank. Then, the air passes through a settling chamber, a contraction nozzle and a developing channel before entering the test section. After leaving the test section, the air is sent through an exhaust portion and discharged into the ambient.

The test section without inclining the bottom plate has a cross-section of 22.5 mm in height and 450 mm in width, providing an aspect ratio of $A = 20$, and has a total length of 450 mm. For the test section with a tilting duct bottom, the exit end of the bottom plate is inclined upward to reduce the duct height so that the aspect ratio of the duct cross-section increases from 20 at the duct inlet to 22.5 for one case and to 30 for another case at the duct exit. Despite the noted change of the duct aspect ratio by the bottom plate inclination, the corresponding inclined angle of the bottom plate is small and is respectively at 0.34° and 0.97° when measured from the horizontal. The side and top walls of the duct are constructed of 10-mm thick transparent acrylic plates to allow for the visualization of vortex flow patterns. The bottom of the test section is a thick flat bakelite plate embedded with a 15-mm thick, high purity circular copper plate of 300 mm in diameter to model a 12-in semiconductor substrate. The upper surfaces of the bakelite and copper plates are kept at the same inclined level so that the air flow does not experience any step when moving over the copper plate. To obtain the uniform plate temperature, the heating elements attached onto the lower surface of the copper plate are divided concentrically into seven semi-circular zones and the heater for each zone is independently controlled by a GW GPC 3030D laboratory power supply. Besides, a mica sheet is placed between the copper plate and heating elements to prevent the electric current leaking to the copper plate.

A good control of the flow condition upstream of the test section is essential in the experiment. More specifically, at the inlet of the experimental loop the working fluid (air) is driven by a 7.5 hp air compressor and sent through a dryer installed with water vapor and oil filters. This dry air then moves into the high-pressure tank. To proceed with the experiment, the air flow is further controlled by a pressure regulator and its volume flow rate is measured by Brooks 5850E and/or 5851E flow controllers both having an accuracy of $\pm 1\%$. These two flow controllers individually operate in the ranges of 0–10 and 0–50 l/min. Through a flexible tube, the air enters the settling chamber, in which four fine-mesh screens, a divergent buffer section, a honeycomb and another four fine-mesh screens are installed in sequence to reduce the turbulence in the air flow. The air turbulence was

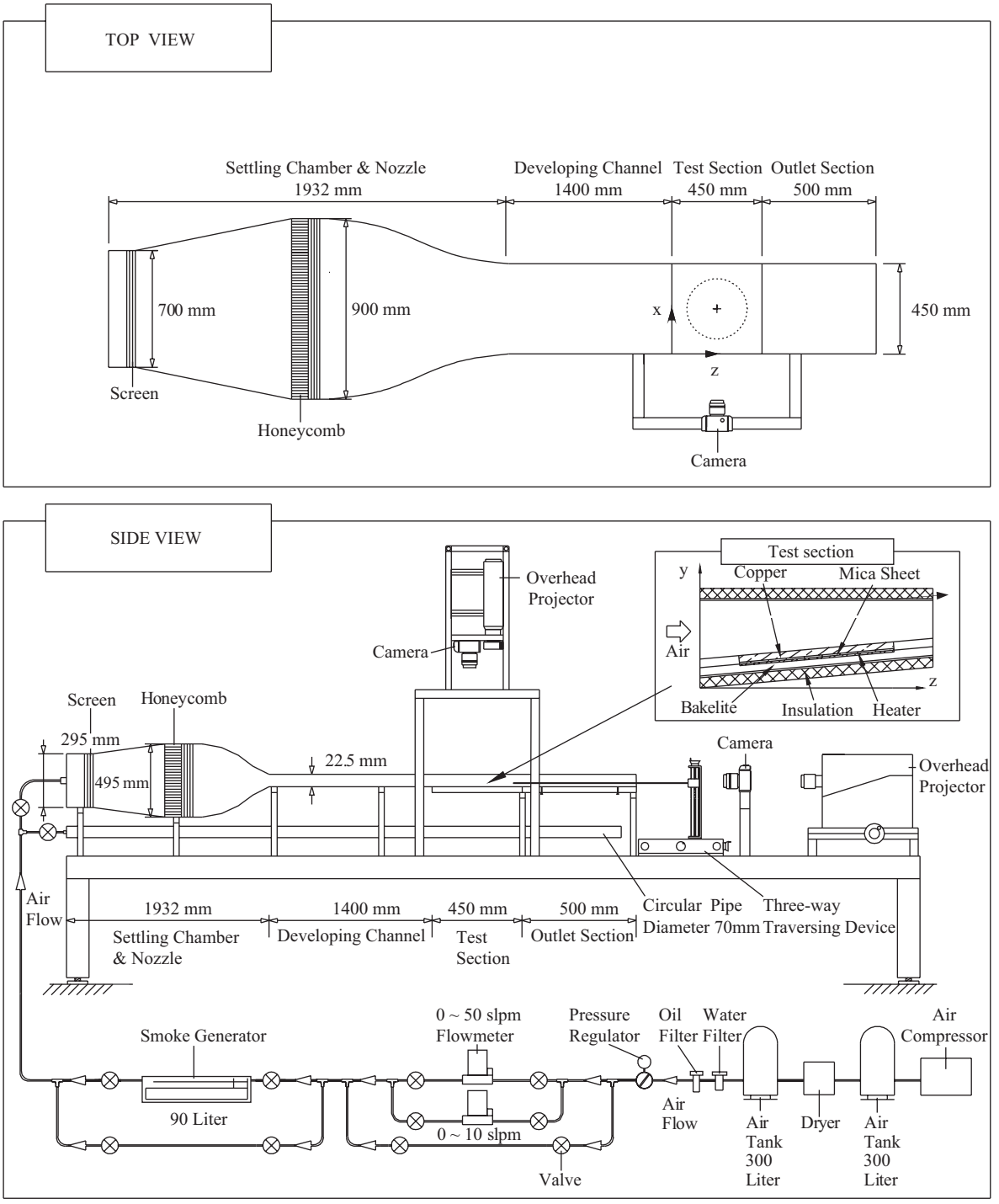

Fig. 1. Schematic of experimental apparatus and the chosen coordinate system for the test section.

further suppressed by passing the air through a contraction nozzle with a contraction ratio of 44:1, which provides a nearly uniform velocity at the inlet of the developing section.

The developing section is 1400 mm in length, approximately 62 times of the duct height. This insures that the flow be fully developed at the inlet of the test section for $Re \leqslant 100$. An insulated outlet section of 500 mm long is added to the test section to reduce the effects of the disturbances from discharging the air flow to the ambient. The developing section and outlet sections are both made of 10-mm thick acrylic plate, whereas the settling chamber and contraction nozzle are made of stainless steel SS-304 plates. The settling chamber, developing section, test section and outlet section are all thermally insulated with a 20-mm thick Superlon insulator and the entire loop is fixed on a rigid supporting frame.

Visualization of the buoyancy-driven vortex flow in the test section is realized by injecting smoke at some distance ahead of the settling chamber. The smoke is produced from a smoke generator, which is a cubic space with the incense burned in it. By keeping the smoke concentration at a suitable level, the incense particles can be illuminated by a plane light sheet from a 550 W overhead projector. With an adjustable knife edge a sharp contrast could be achieved between the duct walls and smoke. The flow photos from the top, side and end views of the test section can then be taken. The exposure time is about $\frac{1}{125\,\mathrm{s}}$ in taking the photos.

The temperature of the heated copper plate is measured by 17 calibrated and electrically insulated *T*-type thermocouples embedded at selected locations in the plate. The thermocouple beads are fixed at about 1 mm from the upper surface of the copper plate through the small holes drilled from the back side of the plate. A *T*-type thermocouple is also used to measure the inlet air temperature at locations just upstream of the test section. The signals from the thermocouples are recorded by the Hewlett-Packard 3852A data acquisition system with a resolution of $\pm 0.05\,^{\circ}\mathrm{C}$.

To measure the temperature distribution of the air flow in the duct, a thermocouple probe is inserted from the downstream end of the test section. The probe is supported by a three-way traversing device. More specifically, the thermocouple probe is an OMEGA (model HYP-O) mini hypodermic extremely small *T*-type thermocouple (33 gauge) implanted in a 1-in long stainless steel hypodermic needle. This movable thermocouple probe can measure the time-average and instantaneous temperature of the flow. The temperature data are recorded when the flow reaches steady or statistically stable state, usually 5–6 h after starting the test. It was noted that in all tests the maximum temperature differences between any two locations in the copper plate were below $0.1\,^{\circ}\mathrm{C}$. The error in the temperature difference between the copper surface and the air at the duct inlet is estimated to be within $\pm 0.1^{\circ}\mathrm{C}$.

The time-average temperature distributions in the air flow are obtained by averaging 1000–3000 sampled data at each detection point. The period of the sampling time may be different for different cases. Most importantly, the period has to be long enough to capture all the slowest temperature oscillations in the air flow. The response time of the thermocouple is about 0.12 s and the sampling rate is about 5 Hz in the transient temperature measurement. This sampling rate is high enough for the present low Reynolds number mixed convection experiment.

For convenience, experiments are designated according to the Reynolds and Rayleigh numbers based on the inlet conditions. In each test the flow controller is first set at the predetermined level to impose a desired, fully developed flow through the entire test section. The power supplies are then turned on to raise the copper disk temperature. Usually, it takes about 3 h for the Rayleigh number to be raised to the test point and another 2 h are needed to maintain the buoyancy-driven recirculating flow at steady or statistically stable state. The steady state is ascertained by insuring that the variation in the instantaneous temperature measured in the flow from each thermocouple be less than $\pm 0.1\,^{\circ}\mathrm{C}$ for a period of at least 25 min. The above choice of the steady-state criterion is in accordance with the fact that the measured background temperature disturbances in the flow are found to be slightly less than $\pm 0.1\,^{\circ}\mathrm{C}$. On the other hand, the statistically stable-state is

considered to be reached when the variation of the time-average temperature in the flow is within $\pm 0.1\,^{\circ}C$ for more than 25 min. After the steady or statistically stable-state is reached, we start the temperature measurement and flow visualization.

2.1. Uncertainty analysis

Uncertainties in the Rayleigh number *Ra*, Reynolds number *Re* and other independent parameters are estimated in the light of the standard procedures proposed by Kline and McClintock [21]. The uncertainties of the thermophysical properties of air are included in the analysis. The fundamental thermophysical properties of the working fluid (air) are $\alpha = 0.22$ (cm^2/s), $\beta = 0.0034$ (1/K), $v = 0.162$ (cm^2/s) and $Pr = 0.74$ at 30 °C and 0.997 bar. The fluid properties are further corrected based on the temperature and pressure detected at the inlet of the test section. In addition, the deviation of temperature among the detecting points in the circular copper plate and the control unsteadiness are also accounted for in the evaluation of the data uncertainties. The analysis shows that the uncertainties of temperature, volume flow rate, dimensions, Reynolds number and Rayleigh number measurements are estimated to be less than 0.15 °C, 1%, 0.05 mm, 3%, and 5%, respectively.

3. Results and discussion

It should be mentioned that at the buoyancy high enough to induce return flow certain types of vortex flows such as the longitudinal (L-), transverse (T-), irregular rolls, etc. can also appear in the duct above the heated disk [3,20]. The longitudinal and transverse vortex flows are, respectively, characterized by the rolls with their rotation axes parallel and perpendicular to the main flow direction [22]. Thus, the effects of the substrate inclination on the vortex flows will also be examined, in addition to the return flow. In this experiment at the duct inlet, the Reynolds number of the flow is varied from 3.7 to 79.7 and the Rayleigh number from 9040 to 24,000 for three inclined angles of the bottom plate 0°, 0.34° and 0.97°. The ranges of the *Re* and *Ra* chosen above are in accordance with those encountered in the real CVD processes [1]. In what follows, the vortex flow characteristics affected by the substrate inclination will be presented first. Then the effects of the substrate inclination on the return flow will be examined.

3.1. Vortex flow affected by substrate inclination

To illustrate the effects of the bottom plate inclination on the vortex flow, a series of top view flow photos taken from the duct with its bottom at different inclined angles are compared in Fig. 2 for $Ra = 11{,}900$ with *Re* reduced from 25.1 to 15.3. The result in Fig. 2(a) indicates that for the duct with a horizontal bottom ($\phi = 0^{\circ}$) we have steady and regular L-rolls at $Re = 25.1$. But as *Re* is reduced to 20.0 and 15.3, the buoyancy-to-inertia ratios are high enough to cause the L-rolls to become somewhat deformed and irregular (Figs. 2(b) and (c)). Now comparing the results in Figs. 2(a), (d) and (g) for the same *Re* of 25.1 but for different ϕ reveals that for a small inclination angle of 0.34° we have a delayed onset of the L-rolls. For an increase of the inclination angle to 0.97° only a number of thermals appear above the heated disk. At the lower *Re* of 20.0 the unstable deformed vortex flow in the duct with $\phi = 0^{\circ}$ (Fig. 2(b)) can be significantly suppressed to become thermals at the larger inclination angle of 0.97° (Fig. 2(h)). But at smaller ϕ of 0.34°, we still have unstable L-rolls in the duct (Fig. 2(e)), although they are nearly regular. Similar trend is noted for the lower *Re* of 15.3, as evident from the results shown in Figs. 2(c), (f) and (i). The unstable longitudinal vortex flow at the small ϕ of 0.34° for $Re = 15.1$ and $Ra = 11{,}900$ is further illustrated in Fig. 3 by showing the top and end view flow photos at selected instants of time at $z = 0.6$ and 0.8. In this figure the time t denotes certain time instant at the statistical state. Note that in the upstream region around $z = 0.6$ the L-rolls are essentially steady. But in the slightly downstream region the L-rolls around the central vertical plane ($x = 0.5$) grow and decay in a certain period of time. Later they may merge and split. The flow in this downstream core region is highly unstable. As

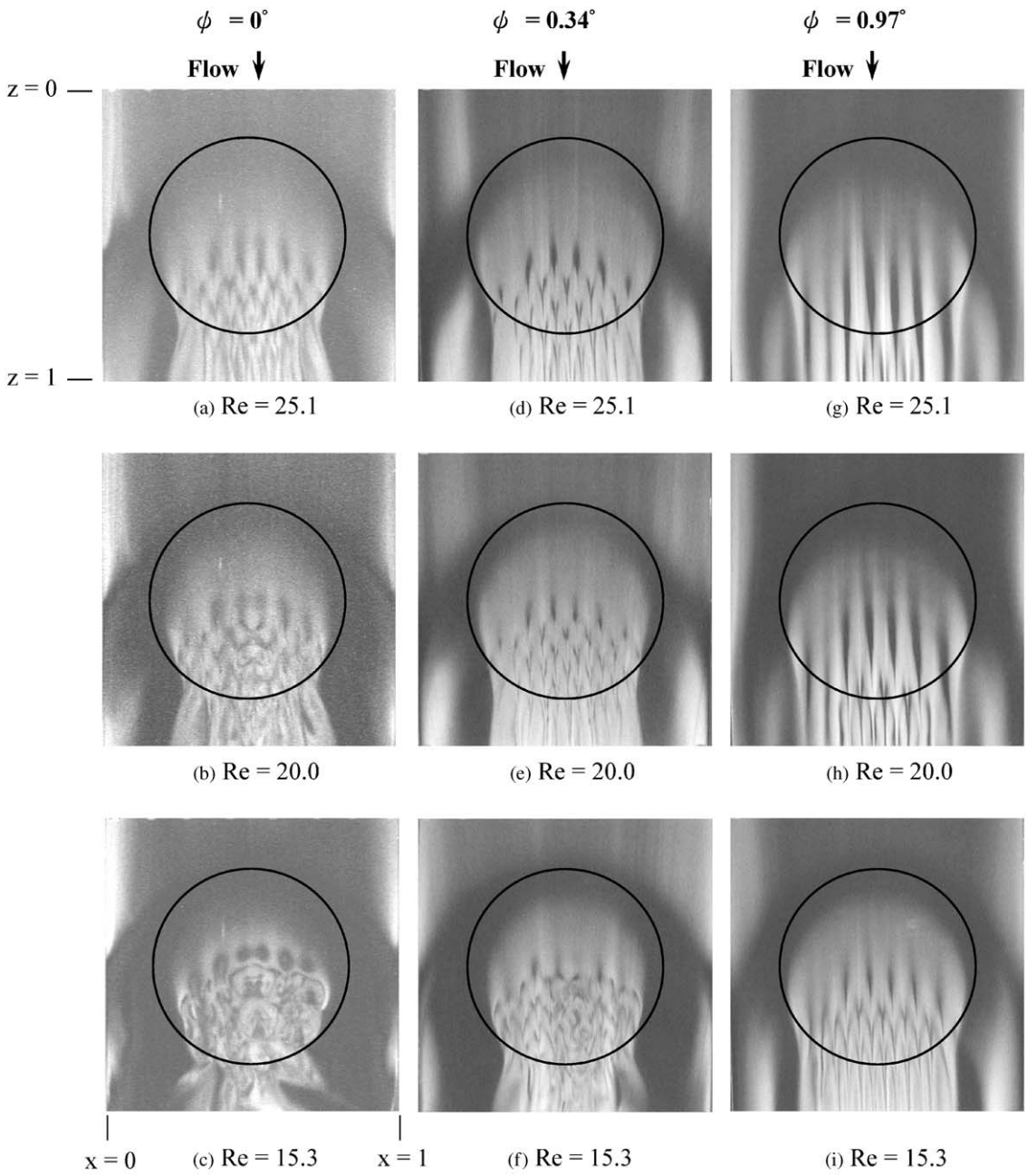

Fig. 2. Top view flow photos of longitudinal vortex flow taken at the plane $y = \frac{1}{2}$ at steady or statistical state in the duct with the duct bottom inclined at 0°, 0.34° and 0.97° for $Ra = 11,900$ at various Reynolds numbers.

the inclination angle is increased to 0.97°, the vortex flow shown in Fig. 4 is characterized by the steady regular L-rolls in the duct.

The effects of the bottom plate inclination on the vortex flow are further shown in Fig. 5 for a higher buoyancy-to-inertia ratio. The regulariza-

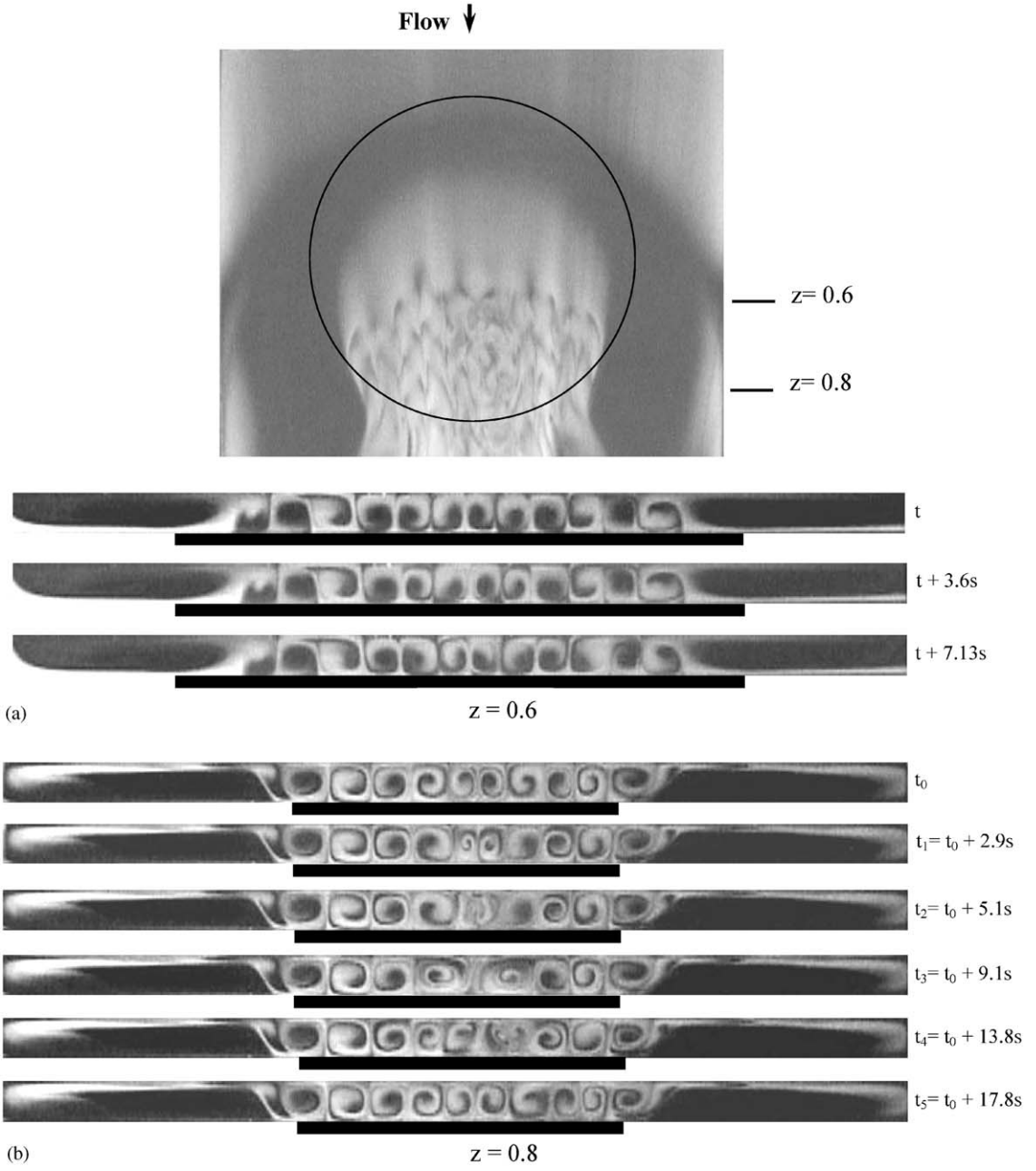

Fig. 3. Top view and end view flow photos of the unstable longitudinal rolls in the duct with $\phi = 0.34^\circ$ taken at the plane $y = \frac{1}{2}$ and at cross-sections $z =$ (a) 0.6 and (b) 0.8 at selected time instants in statistical state for $Re = 15.1$ and $Ra = 11,900$. (The dark bars right below the side view photos signify the location of the heated circular disk).

tion of the unstable deformed longitudinal vortex flow by the main flow acceleration associated with the bottom plate inclination is also clearly seen in Fig. 5 for $Re = 25.1$ and 20.3. It is noted that at the lower Reynolds number for $Re = 15.1$ deformed T-rolls prevail in the rectangular duct with a

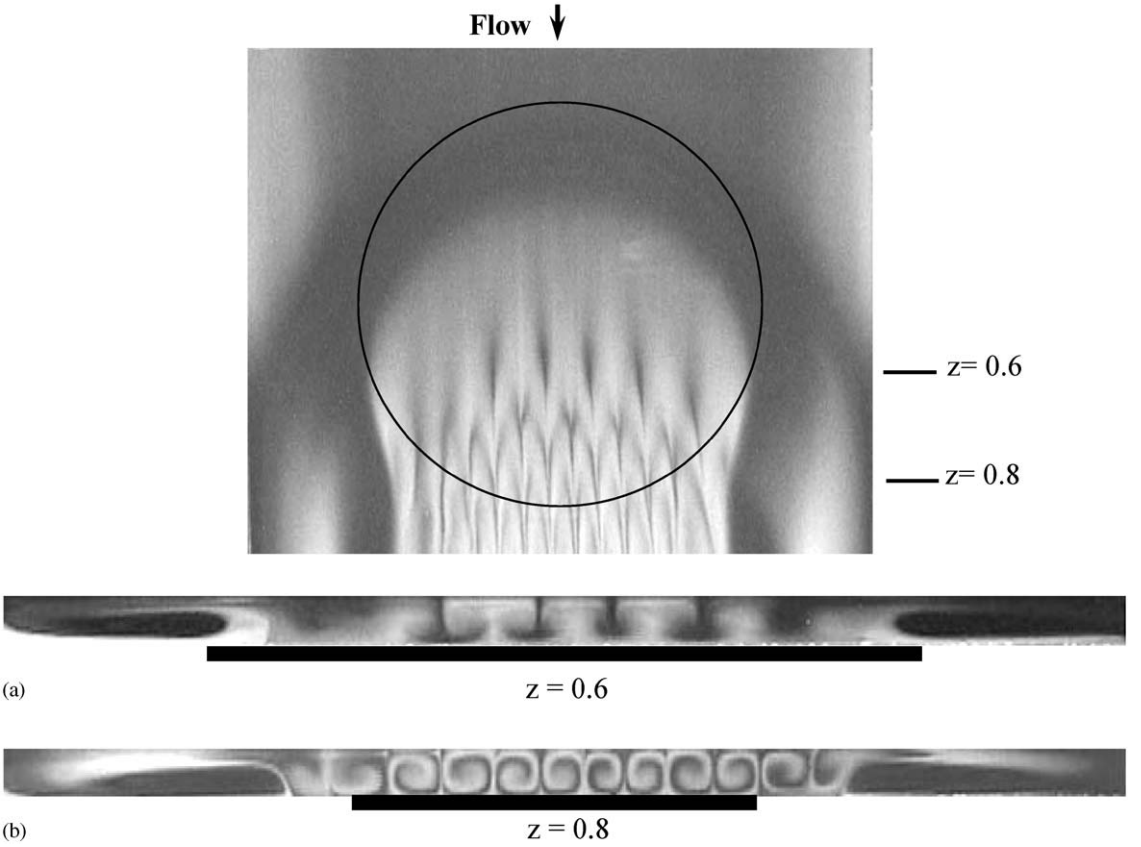

Fig. 4. Top view and end view flow photos of the steady longitudinal rolls in the duct with $\phi = 0.97^\circ$ taken at the plane $y = \frac{1}{2}$ and at cross-sections $z =$ (a) 0.6 and (b) 0.8 for $Re = 15.1$ and $Ra = 11,900$.

horizontal bottom plate ($\phi = 0^\circ$). But when the inclination angle of the bottom plate increases, they break down and slightly asymmetric L-rolls dominate in the duct (Figs. 5(c), (f) and (i)). The stabilization of the longitudinal vortex flow by the inclination of the duct bottom is also clearly seen from the measured time records of the air temperature at selected locations for various Re, Ra and ϕ.

It should be pointed out that an incomplete circular roll appears around the upstream edge of the heated disk, as evident from the top view flow photos in Figs. 2–5. This roll is in fact the buoyancy-induced return flow which was already discussed in our earlier study for $\phi = 0^\circ$ [3]. Note that the return flow driven by the heated circular disk is 3-D.

3.2. Influences of bottom plate inclination on return flow

To illustrate the return flow affected by the bottom plate inclination, the side view flow photos taken at the central vertical plane $x = 0.5$ at the steady or statistically stable-state for $Ra \approx 15,800$ at decreasing Re are presented in Figs. 6 and 7 respectively, for $\phi = 0^\circ$ and 0.97°. The results in Fig. 6 for the horizontal bottom plate indicate that at high Reynolds number with $Re \geqslant 32.1$, the buoyancy-to-inertia ratio Gr/Re^2 is low and no return flow appears in the duct (Figs. 6(a)–(c)). Note that above the downstream half of the heated disk stable L-rolls exist for these cases [3]. As Re is lowered to 27.2, we begin to observe a very small recirculating flow zone in the region near the upper

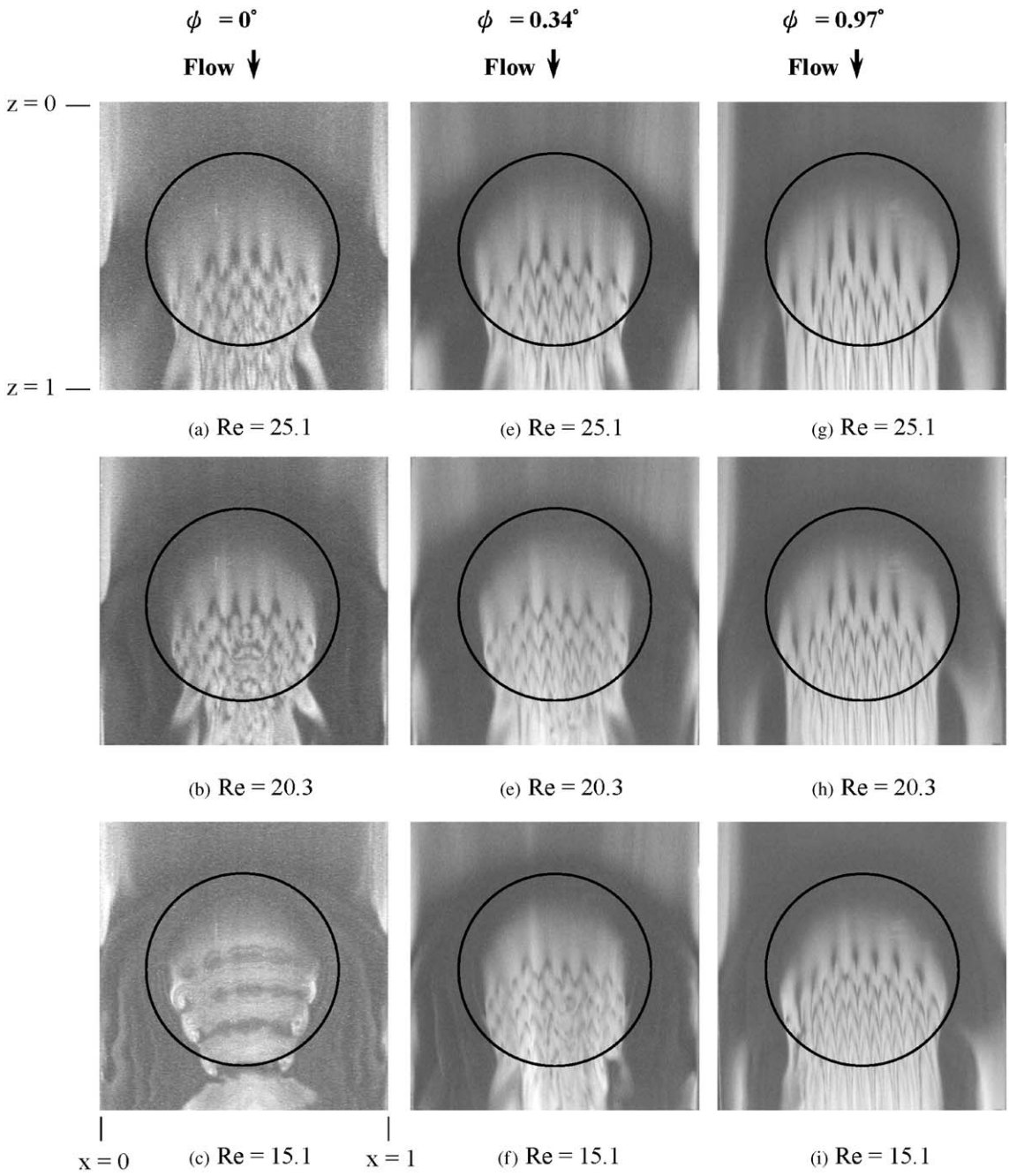

Fig. 5. Top view flow photos of longitudinal vortex flow taken at the plane $y = \frac{1}{2}$ at steady state or at certain time instant in statistical state in the duct with $\phi = 0^\circ$, 0.34° and 0.97° for $Ra = 16,800$ at various Reynolds numbers.

plate in the entrance section of the duct, indicating the onset of the return flow (Fig. 6(d)). A further reduction of the Reynolds number causes the return flow to become stronger and occupies a larger region (Figs. 6(e)–(m)). For the low *Re* of 4.9 and 3.7 the return flow zone is relatively

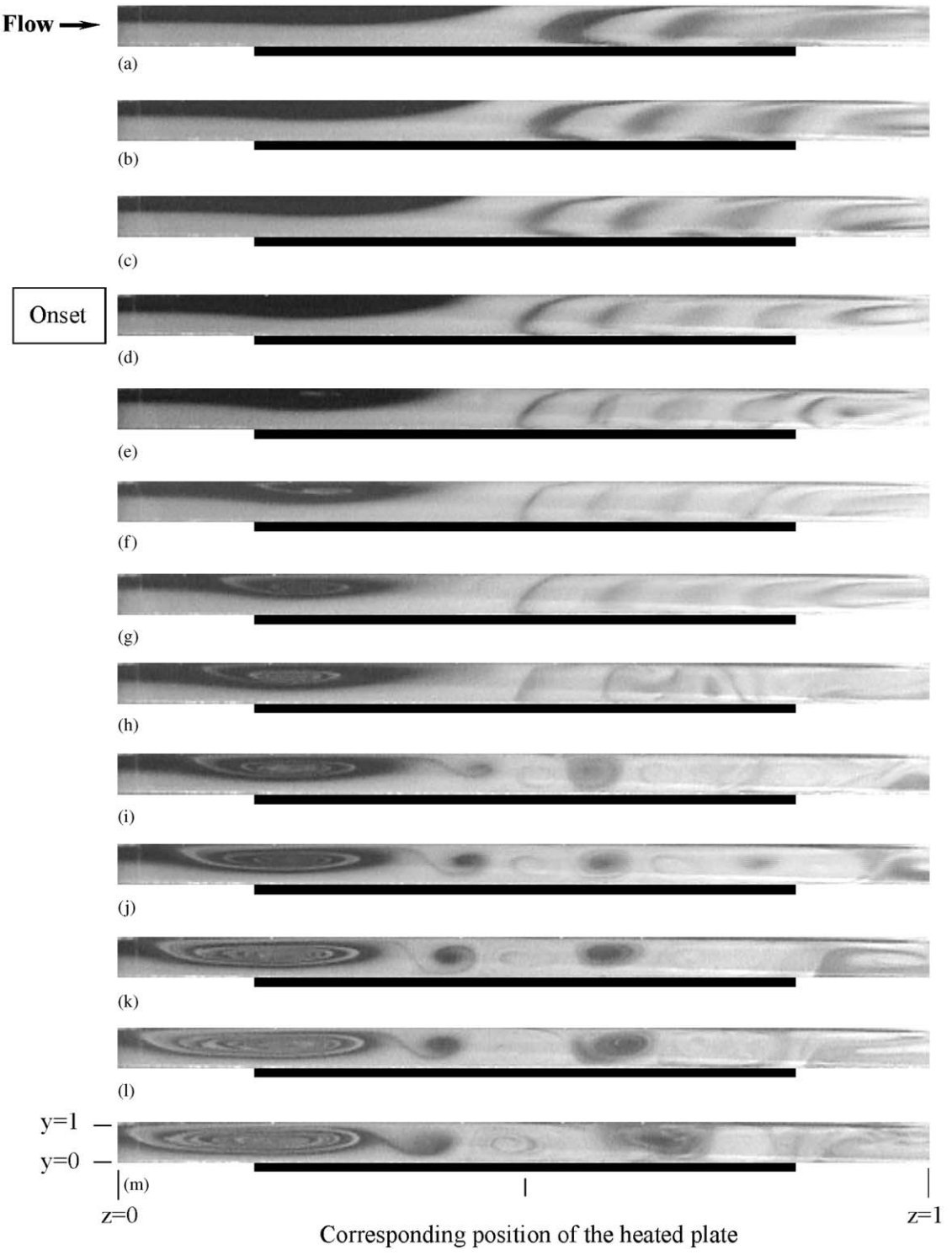

Fig. 6. Side view flow photos taken at the vertical central plane $x = 0.5$ at steady or statistical state for the duct with $\phi = 0^\circ$ for $Ra = 15,800$ for $Re = 39.5$ (a), 34.6 (b), 32.1 (c), 27.2 (d), 24.7 (e), 23.5 (f), 19.8 (g), 14.8 (h), 12.3 (i), 9.9 (j), 7.4 (k), 4.9 (l) and 3.7 (m). (The dark bars right below the side view photos signify the location of the heated circular disk.)

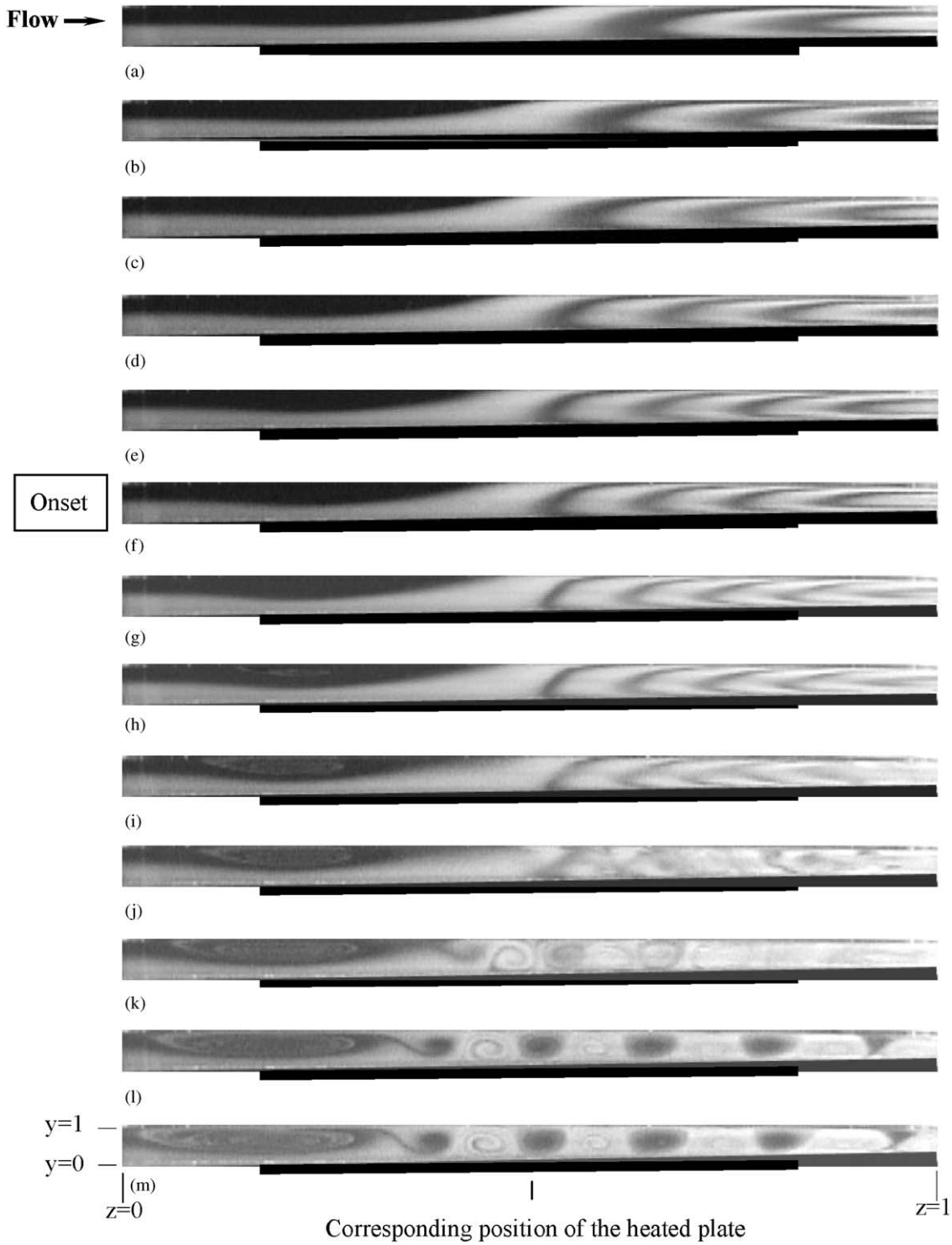

Fig. 7. Side view flow photos taken at the vertical central plane $x = 0.5$ at steady or statistical state for the duct with $\phi = 0.97^\circ$ for $Ra = 15,800$ for $Re = 39.1$ (a), 33.3 (b), 32.1 (c), 27.6 (d), 24.1 (e), 23.1 (f), 20.1 (g), 14.2 (h), 12.5 (i), 9.6 (j), 7.7 (k), 4.2 (l) and 3.3 (m). (The dark bars right below the side view photos signify the location of the heated circular disk.)

large and elongated in the axial direction, which extends deeply into the upstream unheated section (Figs. 6(l) and (m)). Downstream of the return flow zone the duct is dominated by the unstable L-rolls for $19.8 \leqslant Re \leqslant 27.2$ (Figs. 6(d)–(g)) and by T-rolls for $3.7 \leqslant Re \leqslant 9.9$ (Figs. 6(j)–(m)). While for $Re = 12.3$ and 14.8 unstable and somewhat irregular L-rolls and T-rolls dominate in the downstream half of the duct (Figs. 6(h) and (i)). Now when the bottom plate of the duct is inclined at $\phi = 0.97^\circ$, the results in Fig. 7 clearly show that the return flow starts to appear at a lower Re of 21.5 (Figs. 7(f) and (g)), compared with $Re = 27.2$ for $\phi = 0^\circ$. Thus the bottom plate inclination results in a substantial delay in the onset of the return. Moreover, even for the lower Re ($\leqslant 14.2$) with the bottom plate inclined the buoyancy induced return flow in the duct is weaker in intensity and smaller in size (Figs. 7(h)–(m)). The weakening of the return flow by the bottom plate inclination can be more clearly demonstrated by presenting the selected side view flow photos for $\phi = 0^\circ$ and 0.97° together in Fig. 8 at the same Re and Ra. A close inspection of the results in Fig. 8 reveals that the reduction in the size of the return flow zone by the bottom plate inclination is more effective at a higher Re.

The significant increase of the critical buoyancy-to-inertia ratio for the onset of the return flow by the bottom plate inclination is shown in Fig. 9 according to the present data. Note that the critical Gr/Re^2 is almost doubled when ϕ is raised from 0° and 0.97° for all Reynolds numbers tested here. Furthermore, the critical Gr/Re^2 from our

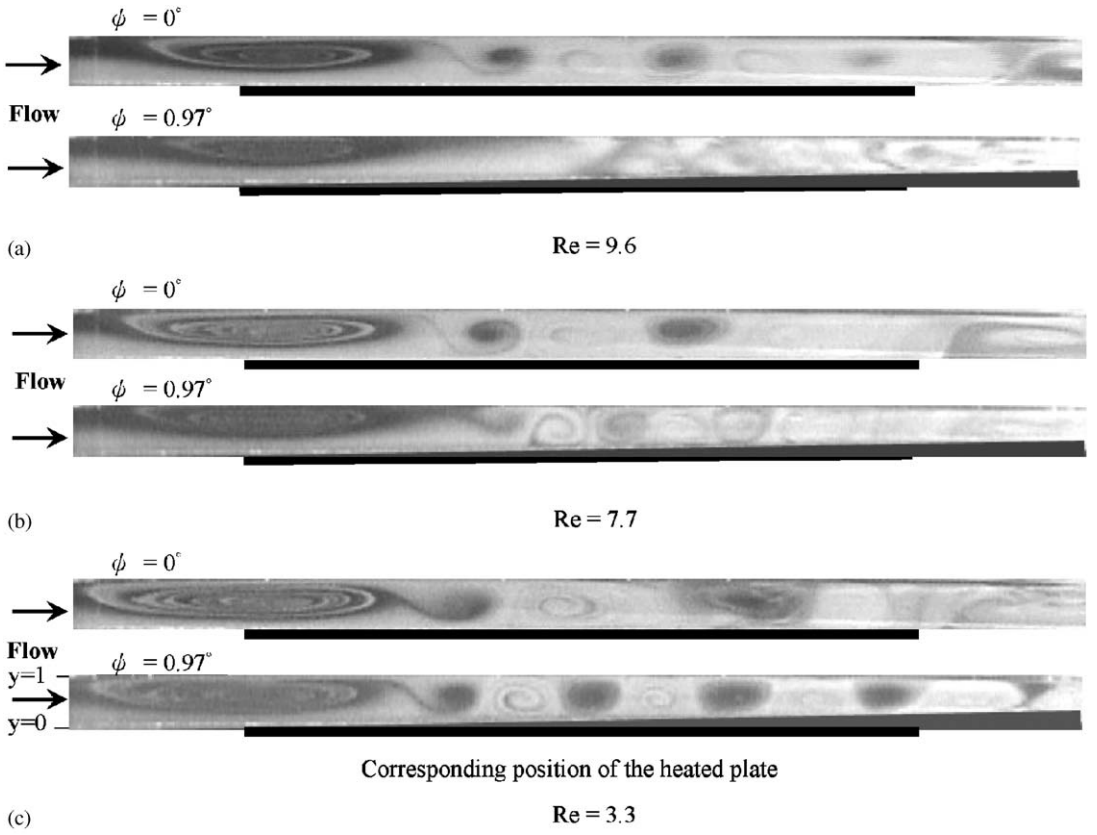

Fig. 8. Side view flow photos taken at the vertical central plane $x = 0.5$ at steady or statistical state in the duct with $\phi = 0^\circ$ and 0.97° for $Ra = 15,800$ at $Re = 9.6$ (a) 7.7 (b) and 3.3 (c). (The dark bars right below the side view photos signify the location of the heated circular disk.)

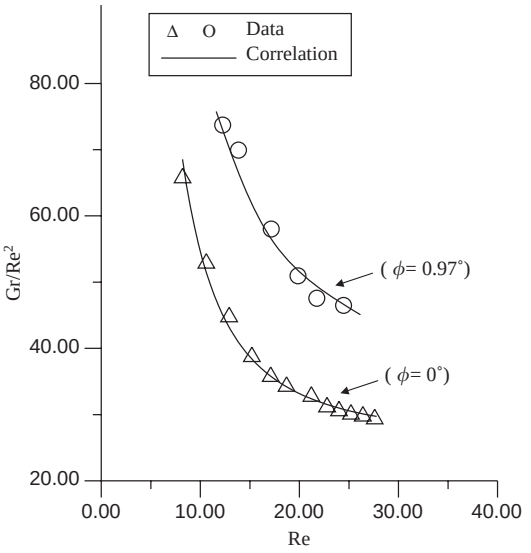

Fig. 9. Critical conditions for the onset of return flow in the duct with $\phi = 0^\circ$ and 0.97°.

experiments can be correlated as

$$Gr/\mathrm{Re}^2 = (26 + 2860/\mathrm{Re}^2)/\cos(44\phi) \quad (1)$$

for $0 \leqslant \phi \leqslant 0.97^\circ$, $7800 \leqslant \mathrm{Ra} \leqslant 21{,}000$ and $12 \leqslant \mathrm{Re} \leqslant 26$. In the above equation the unit of ϕ is in degree. The above correlation is also compared with our data in Fig. 9.

4. Concluding remark

Experimental flow visualization and temperature measurement have been conducted here to explore the effects of the substrate inclination on the buoyancy-induced return flow in mixed convection of gas in model horizontal MOCVD processes. In the experiment, the Reynolds number is varied from 3.7 to 79.7 and Rayleigh number from 9040 to 24,000 for various inclined angles of the bottom plate. The major conclusions obtained here can be summarized as follows:

(1) Due to the acceleration of the main flow by the bottom plate inclination, the buoyancy driven unstable L-rolls and T-rolls can be effectively stabilized by the substrate inclination. Besides, the onsets of longitudinal and transverse vortex rolls are delayed.
(2) The main flow acceleration by the bottom plate inclination noticeably delays the onset of the return flow and weakens it to some degree.
(3) An empirical equation has been proposed to correlate the onset condition of the return flow.

During the course of this investigation, it is recognized that the elimination of the return flow is relatively important in the MOCVD processes. Simple methods to delay and even eliminate the return flow need to be further developed and explored in the future.

Acknowledgements

The financial support of this study by the engineering division of National Science Council of Taiwan, ROC through the contract NSC 89-2212-E009-074 is greatly appreciated.

References

[1] M.L. Hitchman, K.F. Jensen, Chemical Vapor Deposition: Principle and applications, Academic Press, San Diego, 1993 (Chapters 6 and 2).
[2] Y. Mori, J. Heat Transfer (1961) 479.
[3] J.L. Tuh, T.F. Lin, J. Crystal Growth 257 (2003) 199.
[4] F.C. Eversteyn, P.J. Severin, C.H.J. van den Brekel, H.L. Peek, J. Electrochem. Soc. 117 (1970) 925.
[5] Y. Kamotani, S. Ostrach, H. Miao, ASME J. Heat Transfer 101 (1979) 222.
[6] L.J. Giling, J. Electrochem. Soc. 129 (1982) 634.
[7] E.P. Visser, C.R. Kleijn, C.A.M. Govers, C.J. Hoogendoorn, L.J. Giling, J. Crystal Growth 94 (1989) 929.
[8] D.I. Fotiadis, M. Boekholt, K.F. Jensen, W. Richter, J. Crystal Growth 100 (1990) 577.
[9] J. Ouazzani, K.C. Chiu, F. Rosenberger, J. Crystal Growth 91 (1988) 497.
[10] J. Ouazzani, F. Rosenberger, J. Crystal Growth 100 (1990) 545.
[11] E.O. Einset, K.F. Jensen, C.R. Kleijn, J. Crystal Growth 132 (1993) 483.
[12] N.K. Ingle, T.J. Mountziaris, J. Fluid Mech. 277 (1994) 249.
[13] D.B. Ingham, P. Watson, P.J. Heggs, Int. J. Heat Fluid Flow 16 (1995) 202.
[14] D.B. Ingham, P. Watson, P.J. Heggs, Int. J. Heat Mass Transfer 39 (1996) 437.

[15] T.M. Makhviladze, A.V. Martjushenko, Int. J. Heat Mass Transfer 16 (1998) 2529.
[16] K.W. Park, H.Y. Pak, Numerical Heat Transfer 37 (2000) 407.
[17] T.S. Chen, A. Moutsoglou, B.F. Armaly, Numeri. Heat Transfer 5 (1982) 343.
[18] C. Gau, C.W. Liu, T.M. Huang, Win Aung, Int. J. Heat Mass Transfer 42 (1999) 2629.
[19] W.S. Tseng, W.L. Lin, C.P. Yin, C.L. Lin, T.F. Lin, ASME J. Heat Transfer 122 (2000) 58.
[20] J.L. Tuh, T.F. Lin, Int. J. Heat Mass Transfer 46 (2003) 1341.
[21] S.J. Kline, F.A. McClintock, Mech. Eng. 75 (1953) 3.
[22] C.H. Yu, M.Y. Chang, T.F. Lin, Int. J. Heat Mass Transfer 40 (1997) 333.